# 24

# QCD jets

## 24.1 Introduction

We shall focus our discussions for jet productions in $e^+e^-$. More complete discussions can, for example, be found in [52] and the different contributions of the LEP groups at the QCD-Montpellier conference series. The aim is to study final states which do not depend on the identification of particular hadronic channels. High-energy $e^+e^-$ experiments offer a such opportunuity, although many aspects of the analysis can be extended to other processes. We shall consider the parton process:

$$e^+e^- \to \gamma^* \to \bar{q}q \, , \tag{24.1}$$

if one assumes that quarks are produced as free particles. In that case, one obtains, the angular distribution:

$$\frac{d\sigma^{(0)}}{d\cos\theta} = \frac{\pi\alpha^2 Q_q^2}{2s}(1 + \cos\theta) \, , \tag{24.2}$$

which after integration gives the parton model total-cross section:

$$\sigma^{(0)} = \frac{4\pi\alpha^2 Q_q^2}{3s} \, . \tag{24.3}$$

## 24.2 IR divergences: Bloch–Nordsieck and KLN theorems

However, the process in Eq. (24.1) does not exist in practice as the production of quarks is always accompanied by the emission of gluons. Formally, this feature is signalled by the appearance of the IR divergences when one evaluates the QCD radiative corrections given by diagrams in Fig. 24.1.

The IR divergence from the vertex correction is cancelled by the one from soft gluon radiation, which renders the total cross-section finite:

$$\sigma^{(1)} = \sigma^{(0)}\left[1 + \frac{3C_F}{4}\left(\frac{\alpha_s}{\pi}\right)\right] \, , \tag{24.4}$$

241
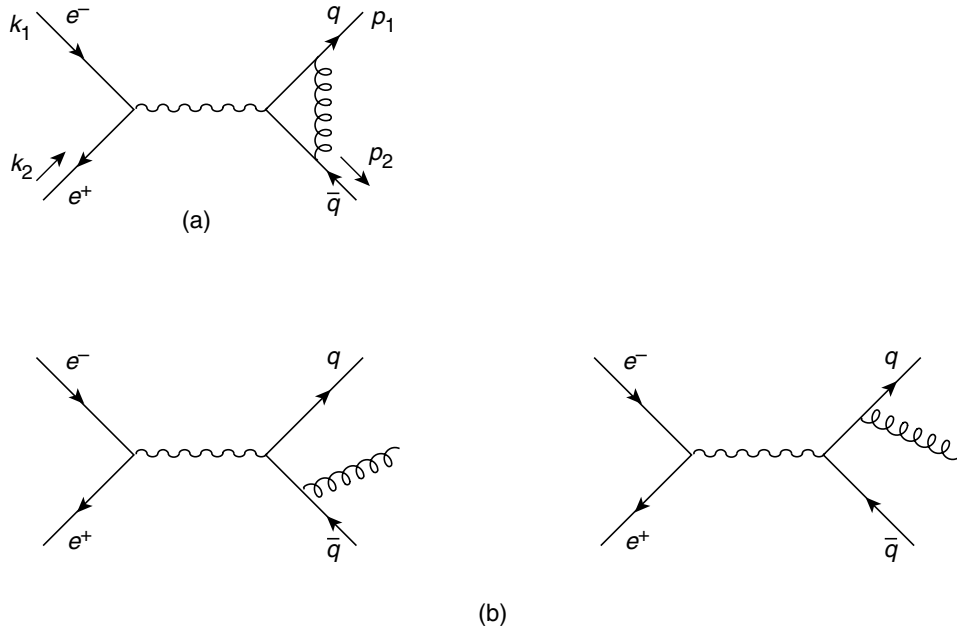
Fig. 24.1. $\alpha_s$ corrections to $e^+e^- \to \gamma^* \to \bar{q}q$. (a) vertex corrections. (b) gluon radiation.

which is the well-known *inclusive cross-section*. Therefore, only the sum of the cross-sections:

$$e^+e^- \to \gamma^* \to \bar{q}q + \bar{q}qg + \cdots \qquad (24.5)$$

is expected to be finite, and this is the quantity that one measures. This cancellation of IR divergence is a general property already encountered in QED for soft and collinear photons and is known as the *Bloch–Nordsieck theorem* [285]. It states that soft divergence is absent for a totally inclusive cross-section. However, new features appear in QCD at higher orders due to the self-gluon interactions, or if one works in a covariant gauge, due to the emission of soft ghosts and the appearance of ghost loops. The theorem has been generalized to QCD by the *Kinoshita–Lee–Nauenberg (KLN) theorem* [286]. The KLN theorem states that in a theory with massless fields, transition rates are free of IR soft and collinear (mass singularities) divergences if the summation over the initial and final *degenerate states* (a massless quark accompanied by an arbitrary number of gluons cannot be distinguished from a single quark) are carried out. That is, for a single-quark state of mass $m$, we should add all final states that in the limit $m \to 0$ have the same mass, including massless gluons and quarks. In order to quantify this feature, one can mimic the IR problem in QED, where, under certain conditions, the processes: $e^+e^- \to \bar{q}q$ and $e^+e^- \to \bar{q}qg, \ldots$ are indistinguishable. This is realized if the gluon energy $k_0$ is below a certain detection threshold or if the angle formed by its three-momentum $\mathbf{k}$ with the quark momenta $\mathbf{p_i}$ is smaller than
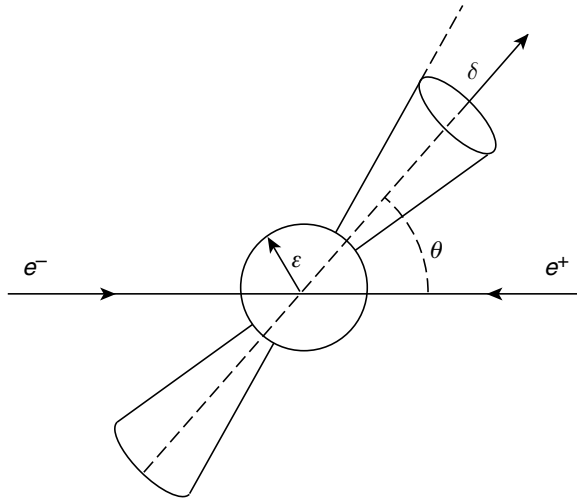
Fig. 24.2. Two 'fat' jets with possible extra soft partons (inside the sphere).

the detector resolution [287]:

$$k_0,\, p_{i0} \leq \epsilon\sqrt{s}$$
$$\angle(\mathbf{k}, \mathbf{p_i})\,,\ \angle(\mathbf{p_1}, \mathbf{p_2}) \leq \delta\,, \tag{24.6}$$

where $\epsilon$ and $\delta$ which characterizes the detection efficiency are defined in Fig. 24.2.

The previous conditions can be generalized for more produced numbers of quarks and gluons. If one considers the massless quark propagator in Fig. 24.2:

$$-\frac{i}{\hat{p}_1 + \hat{k}} \simeq i\frac{\hat{p}_1 + \hat{k}}{2p_1 \cdot k}\,, \tag{24.7}$$

which indicates that for soft partons $k_0,\ p_{i0} \simeq 0$ or for collinear momenta $\mathbf{p_1} \parallel \mathbf{k}$, the denominator vanishes (*collinear mass singularities*). The conditions in Eq. (24.6) guarantee that this does not happen because:

$$p_1 \cdot k \geq \frac{1}{2}s(\epsilon\delta)^2\,, \tag{24.8}$$

which after integration over final particle momenta, corresponds for the cross-section, to the singularity:

$$\sigma_{\text{sing}}^{(1)} \sim \alpha_s \ln\epsilon \ln\delta\,. \tag{24.9}$$

This result informs us that at higher energies this contribution becomes more and more negligible as $\alpha_s$ is smaller, such that the parton model description of the cross-section will be much better and the events are more jet-like. However, the complete analysis is more complicated because we see jets of hadrons (*hadronization*) not quark jets. This leads to the introduction of *fragmentation functions* discussed previously.

Fig. 24.3. Two-jet events seen in $e^+e^-$ at PETRA (1979).

## 24.3 Two-jet events

It is instructive to compare Fig. 24.2 with the two jet events seen inside the detector (Fig. 24.3).

Using the Sterman–Weinberg parametrization, one can explicitly show the different contributions from Fig. (24.2), where each individual contributions are IR divergent, which we regulate by attributing a mass $\lambda$ to the gluons. The contribution of the diagrams in Fig. (24.1b) for the production of a real gluon can be divided into three parts:

- A contribution of a $\bar{q}q$ jet plus a jet due to *a hard gluon inside the cone* with an energy greater than $\epsilon\sqrt{s}$ from Fig. (24.2b), which is:

$$\sigma(\text{hard})^{(b)} = \sigma^{(0)} C_F \left(\frac{\alpha_s}{\pi}\right) \left[-\ln\left(\frac{\delta\sqrt{s}}{\lambda}\right)(3 + 4\ln 2\epsilon) - 2\ln^2 2\epsilon + \frac{17}{4} - \frac{\pi^2}{3} + \mathcal{O}(\epsilon, \delta)\right].$$

(24.10)

- A contribution due to two jets from $\bar{q}q$ and the one due to *a soft gluon inside the cone* with an energy smaller than $\epsilon\sqrt{s}$, which is:

$$\sigma(\text{soft})^{(b)} = \sigma^{(0)} C_F \left(\frac{\alpha_s}{\pi}\right) \left[2\ln^2\left(\frac{2\epsilon\sqrt{s}}{\lambda}\right) - \frac{\pi^2}{6} + \mathcal{O}(\epsilon, \delta)\right].$$

(24.11)

- A contribution from the interference of the lowest order diagram with the vertex and self-energy corrections, which is:

$$\sigma(\text{interf})^{(c)} = \sigma^{(0)}\left[1 + C_F\left(\frac{\alpha_s}{\pi}\right)\right]\left[-2\ln^2\left(\frac{\sqrt{s}}{\lambda}\right) + 3\ln\left(\frac{\sqrt{s}}{\lambda}\right) - \frac{7}{4} + \frac{\pi^2}{6} + \mathcal{O}(\epsilon, \delta)\right] .$$
(24.12)

The sum of the different contributions, where all but a fraction of the total energy is emitted inside these cones, are IR finite (cancellation of soft and collinear singularities) and reads:

$$\sigma = \sigma^{(0)}\left[1 - C_F\left(\frac{\alpha_s}{\pi}\right)\left[(3 + 4\ln 2\epsilon)\ln\delta - \frac{5}{2} + \frac{\pi^2}{3} + \mathcal{O}(\epsilon, \delta)\right]\right] .$$
(24.13)

Therefore, the fraction of events which have all but a fraction $\epsilon$ of their energy in some pairs of cones with half-angle $\delta$ is:

$$R(2\text{jet}) = \frac{\sigma}{\sigma^{(1)}} = 1 - C_F\left(\frac{\alpha_s}{\pi}\right)\left[(3 + 4\ln 2\epsilon)\ln\delta - \frac{7}{4} + \frac{\pi^2}{3} + \mathcal{O}(\epsilon, \delta)\right] ,$$
(24.14)

where $\sigma^{(1)}$ is the inclusive total cross-section to order $\alpha_s$. This expression is valid if $\epsilon$ and $\delta$ are not too small such that perturbation theory is valid [288]. Alternatively, one can take another parametrization (e.g. cylindrical jet picture). Noting that the previous inclusive total cross-section in Eq. (24.4) includes the two- and three-jet events, the two-jet events can be obtained as:

$$\sigma(2\text{jet}) = \sigma^{(1)} - \sigma(\not{2}\text{jet}) .$$
(24.15)

where $\sigma(\not{2}\text{jet})$ does not contain two-jet events. The cross-section for the process:

$$e^+e^- \to \gamma^* \to \bar{q}qg$$
(24.16)

can be obtained from Fig. (24.2). Defining:

$$s = (p_1 + p_2 + k)^2 \quad \text{and} \quad x_i = 2p_{0i}/\sqrt{s} ,$$
(24.17)

one obtains:

$$\frac{1}{\sigma^{(0)}}\frac{d^2\sigma}{dx_1 dx_2} = \frac{C_F}{2}\left(\frac{\alpha_s}{\pi}\right)\frac{x_1^2 + x_2^2}{(1 - x_1)(1 - x_2)} ,$$
(24.18)

with:

$$x_1 + x_2 \geq 1 , \qquad 0 \leq x_i \leq 1 .$$
(24.19)

Using the geometry of the $\bar{q}qg$ produced state given in Fig. 24.4, this process will not be considered as a two-jet event if the angle $\theta$ between the quark momenta is smaller than $\pi - \eta_0$, where $\eta_0$ is the resolution of the detector. Therefore, the not two-jet (three-jet)
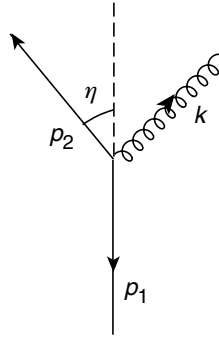
Fig. 24.4. Configuration of $\bar{q}qg$ produced state.

cross-section will be:

$$\sigma(2\text{jet}) = \int^{sup} \int dx_1 dx_2 \frac{d^2\sigma}{dx_1 dx_2} \,, \tag{24.20}$$

where *sup* corresponds to the domain:

$$x_1 + x_2 = 1 + \frac{x_1 x_2}{2}(1 + \cos \eta_0) \,. \tag{24.21}$$

In the limit $\eta_0 = 0$, which corresponds to a much better experimental precision, one obtains:

$$\sigma(2\text{jet}) = \sigma^{(0)} \frac{C_F}{2} \left(\frac{\alpha_s}{\pi}\right) \left[ \ln^2 \frac{4}{\eta_0^2} - 3\ln \frac{4}{\eta_0^2} + \frac{\pi^2}{3} + \frac{7}{2} \right], \tag{24.22}$$

from which one can deduce the observed two-jet total cross-section:

$$\sigma(2\text{jet}) = \sigma^{(0)} \left\{ 1 - \frac{C_F}{2} \left(\frac{\alpha_s}{\pi}\right) \left[ \ln^2 \frac{4}{\eta_0^2} - 3\ln \frac{4}{\eta_0^2} + \frac{\pi^2}{3} + 2 \right] \right\} \,, \tag{24.23}$$

which depends on the resolution $\eta_0$. This result differs from that of Sterman–Weinberg, which shows the dependence of the cross-section on the parametrization of the two-jet event.

## 24.4 Three-jet events

Experimentally, three-jet events have been observed in $e^+e^-$ experiments. We show these events in Fig. 24.5.

It is interpreted in QCD as coming from quark-anti-quark plus a gluon emitted from one of the quark.
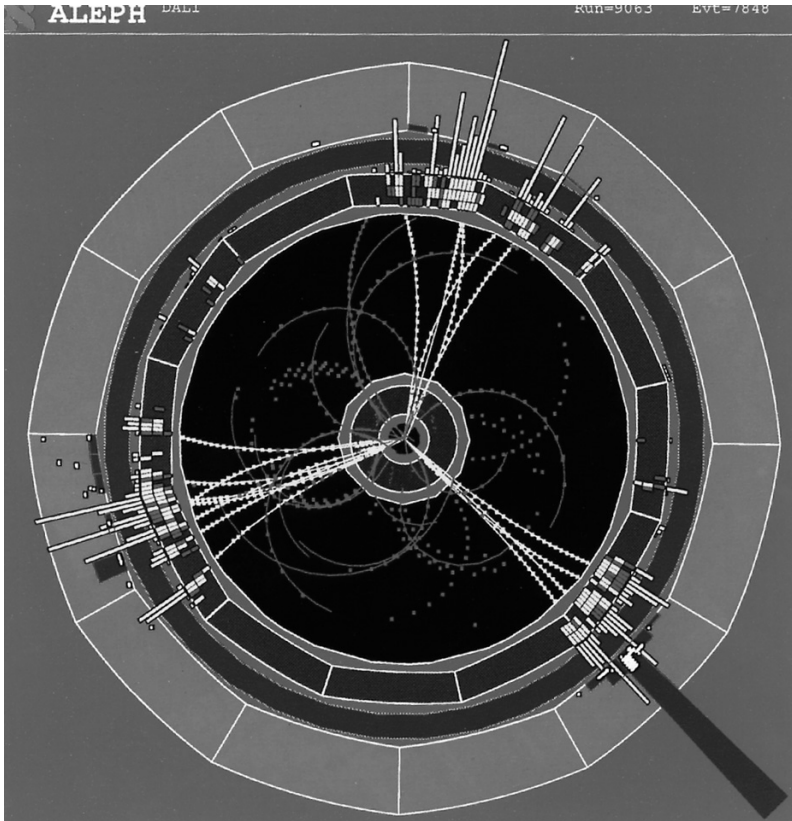
Fig. 24.5. Three-jet events seen at LEP.

The three-jet cross-section has been already evaluated in Eq. (24.20). For studying these events, it is convenient to introduce the kinematic variables:

$$x_1 = 2p_{01}/\sqrt{s} , \qquad x_2 = 2p_{02}/\sqrt{s} , \qquad x_3 = 2k_0/\sqrt{s} = 2 - x_1 - x_2 . \quad (24.24)$$

### 24.4.1 Thrust as a jet observable

Different observables have been proposed in the literature for a qualitative description of final state topology. They are, for example, useful to define the axis or the plane of the event and therefore longitudinal and transverse momentum distributions. These variables should be linear in energy and/or momentum in order to meet the necessary condition of cancellation of IR divergence. *Thrust* and *spherocity* are two alternative IR safe quantities for a parametrization over the continuous range from the topology of a sphere to that of an ideal collinear two-jet event. *Spherocity* is defined as [290]:

$$S = \left(\frac{4}{\pi}\right)^2 \min\left(\frac{\sum_i |\mathbf{p_{i\perp}}|}{\sum_i |\mathbf{p_i}|}\right)^2 , \qquad (24.25)$$

where $\mathbf{p_{i\perp}}$ is the transverse momentum with respect to the minimum direction (spherocity axis). It has the extremal values:

$$0 \le S \le 1 \qquad S = \begin{matrix} 1 : & \text{sphere} \\ 0 : & \text{line} \end{matrix} \tag{24.26}$$

The *thrust* variable is defined as [289]:

$$T = 2\max \frac{\sum |\mathbf{p_{i\|}}|^2}{\sqrt{s}} , \tag{24.27}$$

where the sum runs over all particles in a hemisphere; $\mathbf{p_{i\|}}$ are the components of particle momenta along the jet axis contained in the hemisphere. The plane of the hemisphere is chosen to be perpendicular to the jet axis. The latter is found by requiring $T$ to be maximal. This can be obtained by choosing an arbitrary jet axis characterized by the polar angles $(\theta, \phi)$, and evaluates $T(\theta, \phi)$ as a function of these angles. In terms of partonic variables:

$$T = \max \{x_1, x_2, x_3\} , \tag{24.28}$$

and, in general, it has the boundaries:

$$1/2 \le T \le 1 . \tag{24.29}$$

Integrating the cross-section in Eq. (24.18) at fixed $T$, one finds the differential cross-section:

$$(1 - T) \frac{d\sigma}{dT} = \sigma^{(0)} \frac{C_F}{2} \left(\frac{\alpha_s}{\pi}\right) \left[ \left(6T - 6 + \frac{4}{T}\right) \ln\left(\frac{2T - 1}{1 - T}\right) + 3 \left(3T^2 - 8T + 4\right) \right] , \tag{24.30}$$

The average value is [291]:

$$\langle 1 - T \rangle_{\bar{q}qg} = \frac{C_F}{2} \left(\frac{\alpha_s}{\pi}\right) \left[ -\frac{3}{4} \ln 3 - \frac{1}{18} + 4 \int_{2/3}^{1} \frac{dT}{T} \ln\left(\frac{2T - 1}{1 - T}\right) \right]$$
$$\simeq 1.05 \left(\frac{\alpha_s}{\pi}\right) . \tag{24.31}$$

Another alternative definition of thrust, mostly used at LEP, is:

$$T = \overset{\max}{\mathbf{n}} \frac{\sum_i |\mathbf{p_i} \cdot \mathbf{n}|}{\sum_i |\mathbf{p_i}|} , \tag{24.32}$$

where $\mathbf{p}$ is the momenta of particles produced, while $\mathbf{n}$ is a unit vector. The thrust axis $\mathbf{n_T}$ is the direction at which the maximum is attained.

### 24.4.2 Other event-shape variables

Below we shall list some other event-shape parameters useful in the jet analysis. They are IR safe quantities, i.e. free from IR divergences, which are insensitive to the emission of soft or collinear partons at the logarithmic level.

- **Heavy (resp. light) jet mass** A plane through the origin and orthogonal to the thrust axis $\mathbf{n_T}$ divides the event into two hemispheres $H_1$ and $H_2$, from which one obtains the corresponding normalized hemisphere invariant masses:

$$M_i = \frac{1}{s}\left(\sum_k p_k\right)^2 , \qquad i = 1, 2 , \tag{24.33}$$

where $s \equiv E_{vis}$ is the square of the *total visible energy* of the events. The heavier (resp. lighter) of the two hemispheres is called heavy (resp. light) jet mass $M_h$ (resp. $M_l$).

- **The jet broadening** corresponding to the definition in Eq. (24.32), is defined as:

$$B_k = \left(\sum_{i \in H_k} |\mathbf{p_i} \times \mathbf{n_T}|\right) \Bigg/ \left(2\sum_i |\mathbf{p_i}|\right) . \tag{24.34}$$

- **The total jet broadening** is defined as:

$$B_T = B_1 + B_2 . \tag{24.35}$$

- **The wide jet broadening** is defined as:

$$B_W = \max(B_1, B_2) . \tag{24.36}$$

- The **C parameter** is defined as:

$$C = 3(\lambda_1\lambda_2 + \lambda_2\lambda_3 + \lambda_3\lambda_1) , \tag{24.37}$$

where $\lambda_i$ is the eigenvalue of the quantity:

$$\left(\sum_i \left(p_i^a p_i^b\right)/|\mathbf{p_i}|\right) \Bigg/ \sum_i |\mathbf{p_i}| . \tag{24.38}$$

### 24.4.3 Event-shape distributions

One can generally study any particle distributions in terms of the shape parameters:

$$\mathcal{H}_l = \sum_{k,k'} \frac{|\mathbf{p}(k)||\mathbf{p}(k')|}{s} P_l(\cos \phi_{kk'}) , \tag{24.39}$$

where $s$ is the square of the $e^+e^-$ c.m. energy and $P_l$ is the Legendre polynomials of the angle $\phi_{kk'}$ between two final momenta; $p(k)$ is the final momenta of the particle $k$. In the massless limit, the energy–momentum conservation requires:

$$\mathcal{H}_0 = 1 \quad \text{and} \quad \mathcal{H}_1 = 0 , \tag{24.40}$$

while collinear jets give:

$$\begin{aligned} \mathcal{H}_l &= 1 \quad (l \text{ even}) \\ &= 0 \quad (l \text{ odd}) . \end{aligned} \tag{24.41}$$

In general:

$$0 \leq \mathcal{H}_l \leq \mathcal{H}_0 \, . \tag{24.42}$$

For a continuous distribution of momenta, $\mathcal{H}_l$ corresponds to the multiple momenta:

$$\mathcal{H}_l = \frac{4\pi}{2l+1} \sum_m \left| A_l^m \right|^2 \, , \tag{24.43}$$

where:

$$A_l^m = \int \rho(\Omega) \, Y_l^m(\Omega) d\Omega \, . \tag{24.44}$$

$\Omega$ is the solid angle and:

$$\rho(\Omega) \sim \frac{|\mathbf{p}(k)|}{\sqrt{s}} \, . \tag{24.45}$$

### 24.4.4 Energy-energy correlation

If $\omega$ is an angle between 0 and $\pi$, the energy-energy correlation is defined as [293]:

$$\frac{1}{\sigma^{(0)}} \frac{d\Sigma}{d\cos\omega} = \frac{2}{N_S \Delta\omega \, \sin\omega} \sum_{A=1}^{N} \sum_{\text{pairs in } \Delta\omega} E_{A_a} E_{A_b} \, , \tag{24.46}$$

where $A$ labels the events. In each event, $E_{A_a}$ and $E_{A_b}$ are the energies of two particles separated by an angle $\omega \pm \frac{1}{2}\Delta\omega$. For small resolution $\Delta\omega$, one can impose the conditions:

$$\omega - \frac{1}{2}\Delta\omega \leq \theta_{ab} \leq \omega + \frac{1}{2}\Delta\omega$$
$$\delta(\omega - \theta_{ab})\Delta\omega = \delta(\cos\omega - \cos\theta_{ab})\Delta\omega \sin\omega \, . \tag{24.47}$$

In terms of the partonic variables, one has:

$$\cos\theta_{ab} = \left(x_c^2 - x_a^2 - x_b^2\right)/2x_a x_b \qquad c \neq a, b$$
$$E_a E_b = \frac{s}{4}x_a x_b \, , \tag{24.48}$$

where $a, b, c$ vary from 1 to 3 and $x_3 = 2 - x_1 - x_2$, Substituting into the jet cross-section in Eq. (24.18), one can deduce:

$$\frac{1}{\sigma^{(0)}} \frac{d\Sigma}{d\cos\omega} = \frac{C_F}{2} \left(\frac{\alpha_s}{\pi}\right) \int dx_1 \int dx_2 \frac{x_1^2 + x_2^2}{(1-x_1)(1-x_2)} \sum_{a<b} x_a x_b \delta(\cos\omega - \cos\theta_{ab}) \, . \tag{24.49}$$

After integration, one obtains:

$$\frac{1}{\sigma^{(0)}} \frac{d\Sigma}{d\cos\omega} = \frac{C_F}{8} \left(\frac{\alpha_s}{\pi}\right) \frac{(3-2z)}{z^5(1-z)} [2(3 - 6z + 2z^2) \ln(1-z) + 3z(2-3z)] \, , \tag{24.50}$$

where:

$$z = (1 - \cos \omega)/2 . \tag{24.51}$$

The next order correction to this expression has been evaluated in [294].

### 24.4.5 Jade and Durham algorithms

- **Jade algorithm** Another popular jet definition is the so-called Jade algorithm [295]. For the three jet, one uses the invariant mass cut $y$:

$$s_{ij} = (p_i + p_j)^2 > y_{\text{cut}}s \qquad (i, j = 1, 2, 3) , \tag{24.52}$$

where $s$ is the squared of the sum of the measured energies of all particles of an event. In this original Jade algorithm, one can define:

$$s_{ij} = 2E_i E_j (1 - \cos \theta_{ij}) , \tag{24.53}$$

or the *jet rates*:

$$y_{\text{cut}} = s_{ij}/s , \tag{24.54}$$

where $E_i$ and $E_j$ are the energies of the particles and $\theta_{ij}$ is the angle between them.

- **Durham algorithm** In its variant (Durham and Cambridge algorithms [296]), one defines instead:

$$s_{ij} = 2\min\left(E_i^2, E_j^2\right)(1 - \cos \theta_{ij}) \quad \text{or} \quad y_{\text{cut}} = s_{ij}/s . \tag{24.55}$$

These two definitions are the most used at LEP due to their less sensitivity to hadronization and mass effects.

- **Jet resolution parameter** $y_n$ They are defined as the particular values of $y_{\text{cut}}$ at which events switch from $n - 1$ to $n$-jet configuration.

The QCD expression of the fraction of the three-jet cross-section is of the form:

$$R_3 = \frac{\sigma(3\text{jet})}{\sigma^{(0)}} = \frac{C_F}{2} \left(\frac{\alpha_s}{\pi}\right) \left[ 2\ln^2 \left(\frac{y}{1 - 2y}\right) + 3(1 - 2y)\ln \left(\frac{y}{1 - 2y}\right) \right.$$
$$\left. + \frac{5}{2} - 6y - \frac{9}{2}y^2 + \text{Li}_2 \left(\frac{y}{1 - y}\right) - \frac{\pi^2}{3} \right] \tag{24.56}$$

where:

$$\text{Li}_2(z) \equiv - \int_0^z \frac{dx}{1 - x} \ln x , \tag{24.57}$$

is the dilogarithm function with the properties given in Appendix F. The limit $y = 0$ reflects the IR singularities. The fraction of the two-jet event is:

$$R_2 = 1 - R_3 . \tag{24.58}$$

This result can be generalized for $n$-jet configuration provided that the constraint $s_{ij} > ys$ is satisfied for all $i, j = 1, \ldots, n$. In this case, the pair $i, j$ of particles or cluster of particles

satisfying the previous cut condition is replaced or *recombined* into a single jet or a cluster $k$ with four-momentum $p_k = p_i + p_j$. This procedure is repeated until all pair $y_{ij}$ are larger than the jet resolution parameter cut $y_{cut}$, and the remaining clusters of particles are called jets. One has:

$$R_n = \left(\frac{\bar{\alpha}_s}{\pi}\right)^{n-2} \sum_{j=0} C_j(y)^{C_j^{(n)}} \left(\frac{\bar{\alpha}_s}{\pi}\right)^j , \qquad (24.59)$$

with:

$$\sum_n R_n = 1 . \qquad (24.60)$$

and $\bar{\alpha}_s(s)$ corresponds to the summation of the higher-order term $\alpha_s(v^2)^j \ln^k(s/v^2)$. For large $y$, the jet fractions $R_n$ with $n \geq 3$ are small, while for $y \to 0$, the IR-divergence reappears making the QCD series unreliable. Other jet algorithms in order to improve the QCD predictions at low values of $y$ have been proposed in the literature (see e.g. [297]).

### 24.5 QCD tests from jet analysis

• As we have mentioned previously, one observes jet of hadrons but not jets of quarks or/and gluons. Therefore, one has to take into account the hadronization which is quantified into the fragmentation functions. This effect is modelled through Monte-Carlo analysis and introduces theoretical uncertainties not under control. Jet analyses, like the deep inelastic processes discussed in the previous chapters, have been used to measure the value of the QCD coupling constant where complete results for different energies (91.2, 133, 161, 172, 183, 189 GeV) from LEP studies will be shown in the next chapter. At the $Z_0$ mass, the average results from LEP and SLC are [139]:

$$\alpha_s(91.2 \text{ GeV}) = 0.121 \pm 0.001 \text{ (exp)} \pm 0.006 \text{ (th)} . \qquad (24.61)$$

Recent ALEPH result from four-jets [298] at NLO (order $\alpha_s^3$) leads to:

$$\alpha_s(91.2 \text{ GeV}) = 0.1170 \pm 0.0001 \text{ (stat)} \pm 0.0013 \text{ (syst)} , \qquad (24.62)$$

where the analysis of the error needs to be reconsidered to being convincing.
• Three-jet events are also used to test the gluon spin, where for a spin zero gluon, the term $x_1^2 + x_2^2$ of the cross-section in Eq. (24.18) should be replaced by $x_3^2/4$. The measured distributions agree well with a spin-1 gluon and excludes the spin-0 one.
• One can also notice that the jet event-shape variables are functions of the colour group factors:

$$T_F = 1/2 , \qquad C_F = \left(N_c^2 - 1\right)/(2N_c) , \qquad C_A = N_c , \qquad (24.63)$$

which originate from the $SU(N)_c$ algebra given in Appendix B at the different vertices. Combined fit of these quantities favour the $SU(3)$ group for QCD (see different contributions at the QCD-Montpellier conference). In Fig. 24.6, one compares the scaling violation rates in the hadron spectra
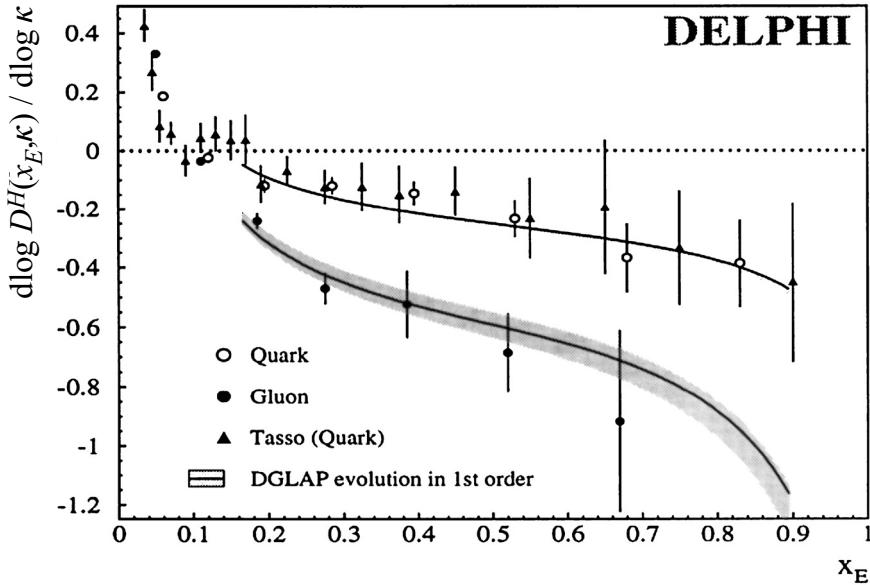
Fig. 24.6. Scaling violation rates in inclusive hadron distributions from
quarks and gluon jets.

from gluon and quark jets as a function of the hardness scale $\kappa$ which caracterizes a given jet [299]. At large $x_E \sim 1$, one expects that the log-derivatives between the quark and gluon jet is close to $C_A/C_F$, which is 9/4 for a $SU(3)_c$ QCD group. As shown in the figure, experimentally, one obtains:

$$\frac{C_A}{C_F} = 2.23 \pm 0.09_{\text{stat}} \pm 0.06_{\text{syst}} . \tag{24.64}$$

In the same way, one expects that hadron multiplicity increases with the hardness of the jets proportional to the multiplicity of secondary gluons and sea quarks. This is shown in Fig. 24.7. The ratio of the slopes in the gluons and quarks jets are proportional to $C_A/C_F$, which is again verified experimentally:

$$\frac{C_A}{C_F} = 2.246 \pm 0.062_{\text{stat}} \pm 0.08_{\text{syst}} \pm 0.095_{\text{th}} . \tag{24.65}$$

## 24.6 Jets from heavy quarkonia decays

Quarkonia decays can also produce gluon jets:

$$
\begin{aligned}
1^{--} &\to 3g \\
&\to 2g\gamma \\
0^{-+} &\to 2g \\
&\to g\gamma
\end{aligned}
\tag{24.66}
$$
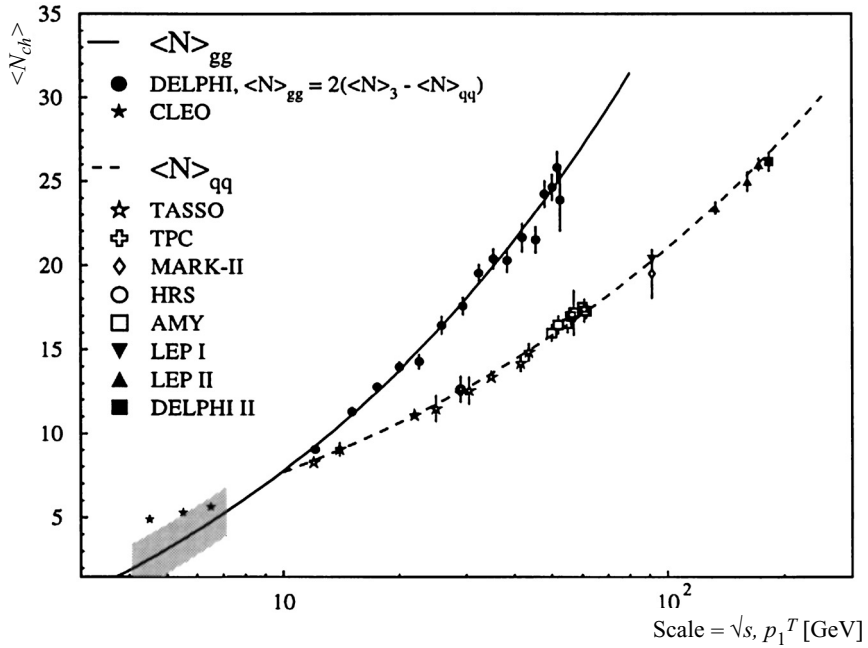
Fig. 24.7. Charged hadron multiplicity in gluons and quark jets.

via OZI violating processes. To leading order, the differential decay rate for $1^{--} \to 3g$, can be written as:

$$\frac{1}{\Gamma_{3g}^{(0)}} \frac{d\Gamma_{3g}}{dx_1 dx_2} = \frac{1}{\pi^2 - 9} \left\{ \left( \frac{1 - x_1}{x_2 x_3} \right)^2 + (x_i \leftrightarrow x_j) \right\} \qquad i, j = 1, 2, 3, \quad (24.67)$$

where $x_i = 2k_i^0 / M_V$, $k_i$ is the gluon momenta and $M_V$ is the vector meson mass. $\Gamma_{3g}^{(0)}$ is the lowest order decay rate:

$$\Gamma_{3g}^{(0)} = \frac{160\alpha_s^3}{81} \frac{|^3 S_1(0)|^2}{M_V^2} , \qquad (24.68)$$

where $|^3 S_1(0)|$ is the wave function at the origin. In terms of the thrust variable, one has [291]:

$$\frac{1}{\Gamma_{3g}^{(0)}} \frac{d\Gamma_{3g}}{dT} = \frac{3}{\pi^2 - 9} \left\{ \frac{4(1 - T)}{T^2(2 - T)^3}(5T^2 - 12T + 8) \ln \frac{2(1 - T)}{T} \right.$$
$$\left. + \frac{2(3T - 2)(1 - T)^2}{T^3(2 - T)^2} \right\}, \qquad (24.69)$$

and the average:

$$\langle T \rangle_{3g} = \frac{3}{\pi^2 - 9} \left\{ 6 \ln(2/3) - \frac{3}{2} + \frac{4\pi^2}{3} + 20 \int_o^1 dx \, \frac{\ln x}{2 + x} \right\} \simeq 0.889 \,. \quad (24.70)$$

## 24.7 Jets from $ep$, $\bar{p}p$ and $pp$ collisions

QCD jets may also be produced in $ep$ or hadronic reactions and from heavy quarkonia decays. In $ep$ scattering, and to leading order in $\alpha_s$, two identified jets in addition to the beam jet from the remnants of the incoming proton, arise from photon gluon fusion and from QCD Compton processes. This process has been also used for determining the QCD coupling $\alpha_s$, where the theoretical uncertainties come from the scale variations and structure functions, while the systematic ones come from the uses of jet algorithms and hadronization models. The result from HERA is [300]

$$\alpha_s(M_{Z^0}) = 0.118 \pm 0.002 \text{ (stat)} \pm 0.008 \text{ (syst)} \pm 0.007 \text{ (th)} \,. \quad (24.71)$$

Jets from hadronic collisions followed the previous strategies used in $e^+e^-$. However, one has to separate *(jet finders)* the jets from the proton remnants from the ones from reconstructed jets, which is different from the case of $e^+e^-$ where all particles are assigned to be jets. At present, one follows the jet definitions used in [301], where jets are defined by concentrations of transverse energy $E_T = |E \sin \theta|$ in cones of radius:

$$R = \sqrt{(\Delta \eta)^2 + (\Delta \phi)^2} \,, \quad (24.72)$$

where $\eta = -\ln \tan(\theta/2)$ is the pseusdorapidity, $\phi$ is the azimuthal and $\theta$ the polar angles of a particle in the calorimeter of the detector, measured with respect of the point of beam crossing. Jets study have been used by the CDF collaboration for determining $\alpha_s$, as a function of $E_T$ and for a radius $R = 0.7$, with the result [302]:

$$\alpha_s(M_{Z^0}) = 0.1178 \pm 0.0001 \text{ (stat)} \, {}^{+0.008}_{-0.010} \text{ (syst)} \, {}^{+0.007}_{-0.005} \text{ (th)} \pm 0.006 \text{ (pdf)} \,, \quad (24.73)$$

where the theoretical error is due to the scale dependence.

Analogously, heavy quark production has been also studied at Tevatron hadron colliders, where there is a good agreement with QCD predictions for the top production, while the total rate and $E_T$ distribution of $b$ quarks produced by CDF exceeds the QCD predictions up to the largest values of $E_T$ by a factor of 3–4. According to [303], this rare discrepancy between the data and QCD predictions can be attributed to the inconsistency of the input $B$ meson fragmentation functions used in previous analysis (mismatch between the perturbative and non-perturbative contributions). This result can be tested in some other processes.